

Molecular Analysis of Potential Hinge Residues in the Inactivation Gate of Brain Type IIA Na⁺ Channels

STEPHAN KELLENBERGER, JAMES W. WEST, WILLIAM A. CATTERALL, and TODD SCHEUER

From the Department of Pharmacology, University of Washington, Seattle, Washington 98195-7280

ABSTRACT During inactivation of Na⁺ channels, the intracellular loop connecting domains III and IV is thought to fold into the channel protein and occlude the pore through interaction of the hydrophobic motif isoleucine-phenylalanine-methionine (IFM) with a receptor site. We have searched for amino acid residues flanking the IFM motif which may contribute to formation of molecular hinges that allow this motion of the inactivation gate. Site-directed mutagenesis of proline and glycine residues, which often are components of molecular hinges in proteins, revealed that G1484, G1485, P1512, P1514, and P1516 are required for normal fast inactivation. Mutations of these residues slow the time course of macroscopic inactivation. Single channel analysis of mutations G1484A, G1485A, and P1512A showed that the slowing of macroscopic inactivation is produced by increases in open duration and latency to first opening. These mutant channels also show a higher probability of entering a slow gating mode in which their inactivation is further impaired. The effects on gating transitions in the pathway to open Na⁺ channels indicate conformational coupling of activation to transitions in the inactivation gate. The results are consistent with the hypothesis that these glycine and proline residues contribute to hinge regions which allow movement of the inactivation gate during the inactivation process of Na⁺ channels.

KEY WORDS: mutagenesis • *Xenopus* oocyte • ion channel • rat

INTRODUCTION

Voltage-gated Na⁺ channels are responsible for initiation of action potentials in neurons and other excitable cells. They are activated by depolarization and are inactivated within ~1 ms by closure of their inactivation gate. Previous results (reviewed in Kellenberger et al., 1997 in this issue) are consistent with the hypothesis that the inactivation gate is formed by the intracellular loop connecting domains III and IV (L_{III-IV}) of the Na⁺ channel α subunit and that a hydrophobic motif (IFM, isoleucine-phenylalanine-methionine)¹ serves as a putative inactivation particle which binds to the intracellular mouth of the pore via hydrophobic interactions and blocks it (West et al., 1992). Based on these studies it was proposed that L_{III-IV} functions as a "hinged-lid" which closes over the intracellular mouth of the pore (Catterall, 1992; West et al., 1992; Eaholtz et al., 1994). By analogy with the structure and function of the hinged lids of allosteric enzymes (Joseph et al., 1990; Wierenga et al., 1991; Derewenda et al., 1992), this model implies that flexible regions on both sides of the IFM motif act as hinges to allow IFM to fold into the

channel structure and bind to a putative inactivation gate receptor in order to latch the inactivation gate in the closed position. Consistent with this hypothesis, previous experiments have provided evidence for movement of the inactivation gate during inactivation. Modification of the inactivation gate by binding of a site-directed antibody (Vassilev et al., 1988; Vassilev et al., 1989) or by reaction of methanethiosulfonate derivatives with a cysteine in the position of the essential F1489 in the IFM motif (Kellenberger et al., 1996) is rapid when the channel is in the resting state but not in the inactivated state, suggesting that the L_{III-IV} moves toward the body of the channel upon inactivation and becomes inaccessible to both macromolecular and small cysteine-modifying reagents.

L_{III-IV} contains several pro and gly residues, amino acids that are components of molecular hinges in other proteins. Gly residues confer flexibility to polypeptides, whereas pro residues induce bends (Creighton, 1993). Thus, gly and pro residues could be components of the hinges in the hinged lid. In these experiments, we tested this idea by analysis of the functional effects of mutations of the pro and gly residues in the inactivation gate. Some of these mutations impaired inactivation by slowing the kinetics of the transition into the inactivated state from closed and open states. In addition, these mutations affected steps in channel gating that occur before channel opening and inactivation, consistent with a firm linkage between conformational changes in L_{III-IV} and those involved in the voltage-dependent channel activation process.

James W. West's present address is Zymogenetics Corp., 1201 Eastlake Ave., Seattle, WA 98102.

Address correspondence to Dr. Todd Scheuer, Department of Pharmacology, Box 357280, University of Washington, Seattle WA 98195-7280. Fax: 206-543-3882; E-mail: scheuer@u.washington.edu

¹Abbreviations used in this paper: IFM, isoleucine-phenylalanine-methionine; IVS3, third transmembrane segment in domain IV; L_{III-IV}, linker between domains III and IV; P_o, open probability; WT, wild type.

MATERIALS AND METHODS

The experimental procedures used in this study are described in Kellenberger et al. (1997) in this issue.

RESULTS

Effects of Mutations of Glycine Residues in the Inactivation Gate

To examine the functional role of gly residues in the inactivation gate, we mutated each gly in L_{III-IV} (SCHEME 1) individually to ala and, in some cases, to val or pro. In addition the double mutation GG1484/5AA was made.

1480-KKKFGGQDIFMTEEQKKYNNAMKKLG-SKKPQKPIPRPANKFQGMVF-1525

(SCHEME 1)

The time course of inactivation of each mutant channel was analyzed using cell-attached macropatches and compared to wild type (WT). Averaged current traces from several experiments ($n = 3-16$) at four different test potentials are displayed in Fig. 1. The values for the time constant for macroscopic inactivation, τ_h , at a range of membrane potentials and the extent of steady-state inactivation as a function of membrane potential are plotted in Fig. 2 for selected mutants. The membrane potentials at which half-maximal activation and

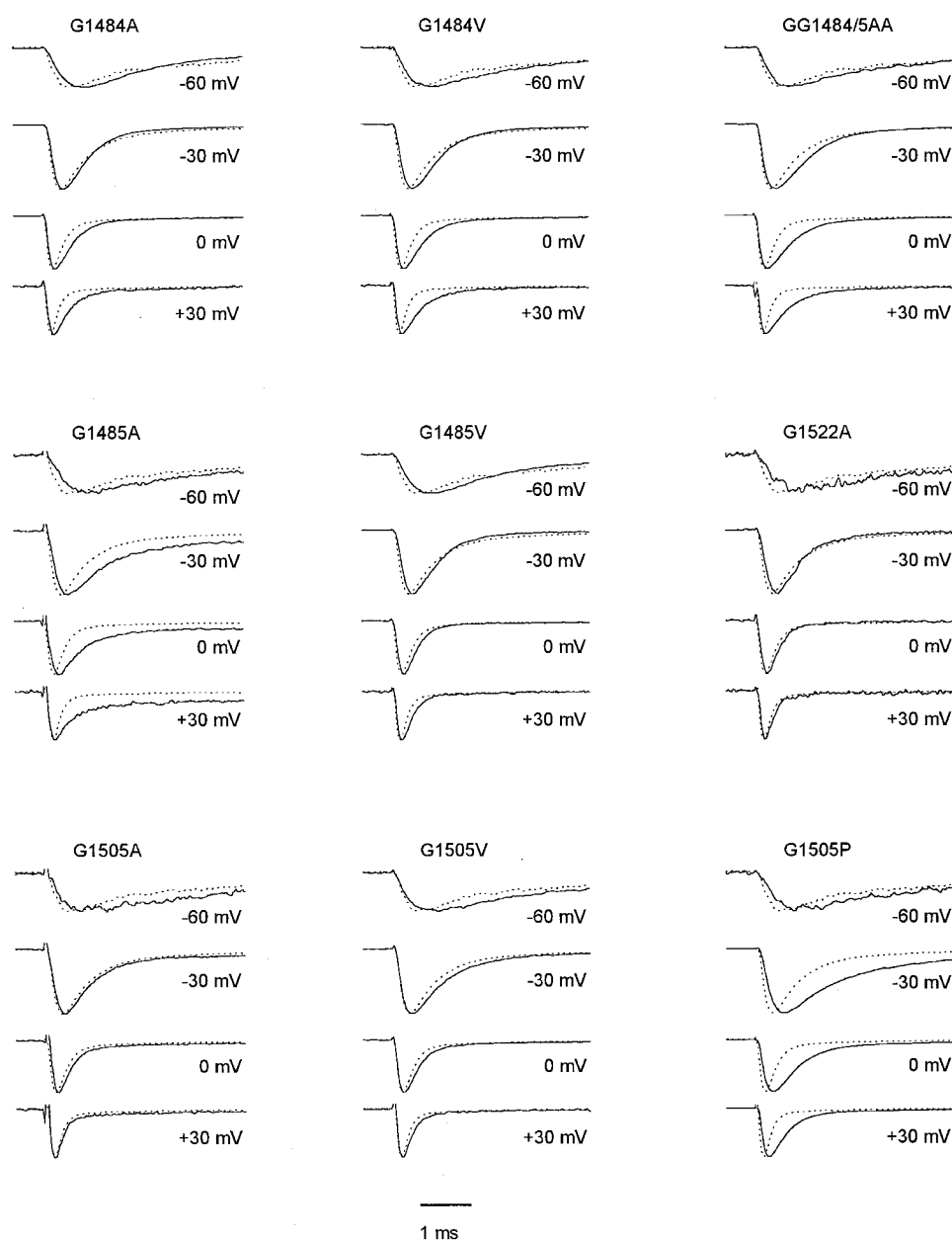


FIGURE 1. Average macropatch current traces from Na⁺ channels with mutated glycine residues. Current traces elicited by depolarizations to the indicated potentials from different experiments were normalized and averaged. WT (dotted lines, $n = 13$ experiments) and mutants (solid lines, $n = 3-8$).

steady-state inactivation were observed are presented in Table I, and mean and SEM values of τ_h at +30 mV are indicated in Table II.

Among the gly residues studied, the largest effects were observed for substitutions of G1484 and G1485 toward the NH₂-terminal end of L_{III-IV}. Both G1484A and G1484V slowed macroscopic inactivation at potentials positive to -30 mV (Figs. 1 and 2 A, Table II). G1485A slowed macroscopic inactivation at all potentials tested (Figs. 1 and 2 A, Table II), and inactivation was incomplete (Fig. 1, Table I). In the macropatches studied here, the fraction of sustained current at the end of 11-ms pulses was $8 \pm 3\%$ for G1485A in comparison to $2 \pm 1\%$ in WT. In contrast, mutation G1485V slowed macroscopic inactivation only slightly, although significantly (Fig. 1, Table II). The double mutant GG1484/5AA slowed macroscopic inactivation to an extent similar to the single G1485A mutation (Fig. 1, Table II), but there was no clear increase in effect for the double mutation. Moreover, the non-inactivating current associated with the G1485A single mutation was absent in the double mutant ($3 \pm 1\%$ noninactivating current, $n = 5$). Thus, the impairment of stability of the inactivated state in the G1485A channel is compensated by the additional G1484A mutation.

Macroscopic inactivation was not affected by mutation G1505A, and was slightly slowed by G1505V (Fig. 1, Table II). However, it was slowed dramatically in mutant G1505P (Fig. 1, Table II). This mutation also caused slowed macroscopic activation. Mutation G1522A at the

COOH-terminal end of L_{III-IV} did not have a significant effect on the inactivation time course.

The mutations of gly residues caused little change in the voltage dependence of activation (Table I). However, the midpoint of steady-state inactivation was shifted positively by mutations G1484A, G1484V, and GG1484/5AA by 7–14 mV (Fig. 2 B, Table I). Steady-state inactivation is primarily a measure of inactivation from closed states without prior channel opening (see DISCUSSION), so these effects suggest that the closed-to-inactivated transition is also impaired by these mutations. Recovery from inactivation after repolarization to negative membrane potentials was not significantly accelerated for these mutants, except for a small effect of G1522A (Table III).

Effects of Mutations of Proline Residues in the Inactivation Gate

Each of the 4 pro residues in L_{III-IV} (SCHEME 1) was mutated, one at a time, to ala, and in addition the triple mutation PPP1512/4/6AAA was made. Of the single mutations the largest effect on current time course was observed in mutant P1512A. This mutation slowed inactivation markedly at all voltages (Figs. 3 and 4 A, Table II). However, the effect was greatest at potentials negative to 0 mV, in contrast to the gly mutations for which effects became stronger with increasing depolarization. Mutation P1512A had little effect on the fraction of non-inactivating current ($4 \pm 1\%$ in macropatches). In addition to its effects on macroscopic inactivation,

TABLE I
Voltage-dependent Gating Parameters of Macroscopic Currents from Mutant and WT Na⁺ Channels

	Peak conductance				Fast inactivation		
	V _{1/2} (mV)	k (mV)	Sustained current (%)	n	V _{1/2} (mV)	k (mV)	n
G1484A	-17 ± 2	-5.2 ± 0.2	2 ± 1	4	-43 ± 1*	5.3 ± 0.2	4
G1484V	-16 ± 2*	-6.1 ± 0.5	3 ± 2	5	-36 ± 1*	4.8 ± 0.1	4
G1485A	-15 ± 2*	-6.7 ± 0.2	8 ± 3*	14	-50 ± 3	6.5 ± 0.2	12
G1485V	-21 ± 4	-6.0 ± 0.5	2 ± 1	3	-47 ± 0	6.1 ± 0.3	3
GG1484/5AA	-19 ± 1	-5.0 ± 0.2	3 ± 1	7	-40 ± 2*	5.4 ± 0.3	13
G1505A	-18 ± 3	-5.7 ± 0.6	1 ± 0	4	-47 ± 2	6.4 ± 0.2	3
G1505V	-22 ± 3	-5.2 ± 0.9	2 ± 1	3	-48 ± 4	6.3 ± 0.1	3
P1509A	-17 ± 2	-7.3 ± 0.6	4 ± 3	4	-55 ± 4*	6.7 ± 0.5	4
P1512A	-22 ± 3	-3.9 ± 0.4	3 ± 2	4	-40 ± 2*	6.5 ± 0.1	4
P1514A	-19 ± 1	-5.9 ± 0.6	2 ± 0	3	-50 ± 1	6.7 ± 0.1	3
P1516A	-15 ± 1*	-7.3 ± 0.3	2 ± 1	3	-50 ± 1	6.3 ± 0.3	3
PPP1512/4/6AAA	-19 ± 1	-5.2 ± 0.2	3 ± 0	7	-42 ± 1*	6.3 ± 0.2	8
A1517G	-24 ± 1*	-4.5 ± 0.3	2 ± 0	4	-52 ± 2	5.8 ± 0.3	3
G1522A	-18 ± 2	-6.2 ± 0.6	2 ± 0	3	-51 ± 1	5.9 ± 0.1	3
WT	-20 ± 3	-5.5 ± 0.3	2 ± 1	8	-50 ± 4	6.2 ± 0.2	7

Values for V_{1/2}, the voltage of half activation or inactivation and the slope factor k were derived from Boltzmann fits to activation and inactivation curves (see MATERIALS AND METHODS, Kellenberger et al., 1997, in this issue); n, number of cells studied. Prepulse duration in steady-state inactivation protocols was 100 ms. All data are from two-electrode voltage-clamp experiments. *V_{1/2} or sustained current significantly different from WT (P < 0.05).

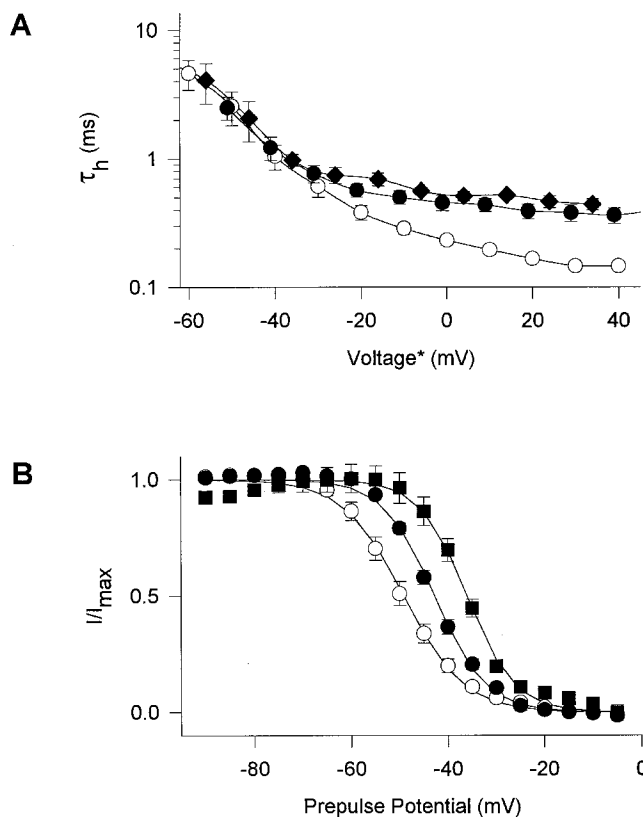


FIGURE 2. Voltage dependence of macroscopic inactivation properties of glycine mutants. (A) Voltage dependence of macroscopic inactivation. τ_h was determined from single exponential fits to the current decay in macropatch experiments. Average values from 4 to 11 experiments are shown for WT (\circ), G1484A (\bullet) and G1485A (\blacklozenge). *The voltage for τ_h values of mutant channels was corrected for differences in the mean midpoints of activation curves relative to WT, to normalize for effects of activation voltage on τ_h . $\Delta V_{1/2}$ relative to WT in macropatch experiments was -9 mV (G1484A) and $+6$ mV (G1485A). (B) Steady-state inactivation curves in response to 100-ms pulses. Data are averages of 4-7 two-electrode voltage-clamp experiments (Table I) with WT, (\circ), G1484A, (\bullet), and G1484V, (\blacksquare). Solid lines are least-square fits of the Boltzmann equation to the data.

P1512A also slowed the time course of macroscopic activation (Fig. 3). This effect may be secondary to the slowing of inactivation at negative membrane potentials in this mutant.

Mutation P1516A slowed inactivation at all potentials tested, but its effects were smaller than those of P1512A (Fig. 3). Mutation P1514A slowed macroscopic inactivation slightly but significantly (Fig. 3, Table II). Macroscopic inactivation of the triple mutant PPP1512/4/6AAA was not significantly different from the single mutation P1512A. In the mutant P1509A, macroscopic inactivation was faster than in WT at potentials negative to 0 mV and not significantly different at more positive potentials (Figs. 3 and 4 A). The different voltage de-

TABLE II
Inactivation Time Course in Cell-attached Macropatches at $+30$ mV

	$\tau_{h(+30\text{ mV})}$	n		$\tau_{h(+30\text{ mV})}$	n
G1484A	0.34 ± 0.04	5	P1509A	0.15 ± 0.01	3
G1484V	0.43 ± 0.04	4	P1512A	0.30 ± 0.03	14
G1485A	0.50 ± 0.03	4	P1514A	0.19 ± 0.01	10
G1485V	0.23 ± 0.02	4	P1516A	0.23 ± 0.01	7
GG1484/5AA	0.50 ± 0.03	5	PPP1512/4/6AAA	0.35 ± 0.03	8
G1505A	0.18 ± 0.02	4	A1517G	0.13 ± 0.01	3
G1505V	0.20 ± 0.01	10	G1522A	0.18 ± 0.01	3
G1505P	0.39 ± 0.03	5	WT	0.16 ± 0.01	13

$\tau_{h(+30\text{ mV})}$ was derived from single exponential fits to the inactivation time course. $\tau_{h(+30\text{ mV})}$ was significantly different from WT ($P < 0.05$) for all mutants tested except for G1505A, P1509A, A1517G, and G1522A.

pendence of macroscopic inactivation in these pro mutants is considered in the DISCUSSION.

The mutations of pro residues caused little change in the voltage dependence of activation (Table I). However, the midpoint of steady-state inactivation was shifted 10 and 8 mV positively by the mutations P1512A (Fig. 4 B, Table I) and PPP1512/4/6AAA (Table I), respectively, suggesting impairment of transitions from closed to inactivated states. Recovery from inactivation was slowed for mutants P1514A, P1516A, and PPP1512/4/6AAA, but not for the other pro mutants (Table III). The slowing of inactivation for mutants P1514A and P1516A occurred without effects on the voltage dependence of activation or steady-state inactivation.

Single Channel Gating of the G1484A, G1485A, and P1512A Mutants

Mutations of G1484, G1485, and P1512 had the most pronounced effects on macroscopic inactivation during depolarizing pulses. Single channel current traces and ensemble averages of mutants to that of these channels at -20 mV are shown in Fig. 5. The ensemble averages (final sweep for each mutant, *solid traces*) were derived from all single channel traces analyzed for each channel type. Their time course corresponds well with the macropatch current traces recorded from the corresponding mutants (Figs. 1 and 3). Thus, the behavior of these single channels is representative of the overall behavior of the channels conducting the macroscopic currents we have measured.

In response to the majority of depolarizations these mutant channels opened once or twice early in the depolarization and then inactivated (Fig. 5), similarly to WT channels (see Kellenberger et al., 1997, in this issue). Sometimes, however, inactivation was delayed or absent, and the single channels had a much higher probability of being open (P_o) late in the pulse. The exact pattern of this high P_o activity varied among mu-

TABLE III
Recovery from Inactivation in Two-electrode Voltage-clamp Experiments

	$\tau_{-60\text{mV}}(\text{ms})$	n	$\tau_{-90\text{mV}}(\text{ms})$	n	$\tau_{-120\text{mV}}(\text{ms})$	n
G1484A	12.72 ± 1.16	3	1.87 ± 0.24	3	$0.51 \pm 0.04^*$	3
G1484V					$0.51 \pm 0.03^*$	3
G1485A	14.28 ± 0.67	4	2.70 ± 0.21	4	0.82 ± 0.05	4
G1485V	18.20 ± 0.67	2	3.57 ± 1.14	2	0.84 ± 0.10	2
GG1484/5AA	15.08 ± 0.86	4	2.31 ± 0.08	4	0.72 ± 0.04	4
G1505A	$10.79 \pm 1.29^*$	2	2.14 ± 0.39	2	$0.54 \pm 0.03^*$	2
G1505V	14.63 ± 1.40	2	1.90 ± 0.26	2	$0.55 \pm 0.03^*$	2
P1509A	14.48 ± 1.10	3	3.12 ± 0.08	3	$0.96 \pm 0.07^*$	3
P1512A	19.07 ± 0.93	3	2.83 ± 0.11	3	0.78 ± 0.01	3
P1514A	21.47 ± 0.25	3	$3.42 \pm 0.03^*$	3	$1.19 \pm 0.13^*$	3
P1516A	22.11 ± 1.27	3	$3.58 \pm 0.08^*$	3	$0.99 \pm 0.05^*$	3
PPP1512/4/6AAA	21.91 ± 0.43	3	$3.41 \pm 0.11^*$	4	$0.92 \pm 0.03^*$	4
A1517G	24.00 ± 1.61	2	3.51 ± 0.41	3	$1.09 \pm 0.02^*$	2
G1522A	$24.36 \pm 1.08^*$	3	$3.95 \pm 0.21^*$	3	0.95 ± 0.10	3
WT	17.66 ± 1.42	4	2.51 ± 0.22	4	0.72 ± 0.03	4

The time course of recovery from inactivation at the potentials indicated was measured after a 15-ms depolarization to 0 mV and fitted with an equation including a single exponential component and a delay (see MATERIALS AND METHODS, Kellenberger et al., 1997, this issue). *Significantly different from WT ($P < 0.05$).

tants (see trace 3 for each mutant in Fig. 5). Because of the unusually high P_o during these depolarizations, relatively few sweeps of this type can potentially have pronounced effects on the macroscopic current. There-

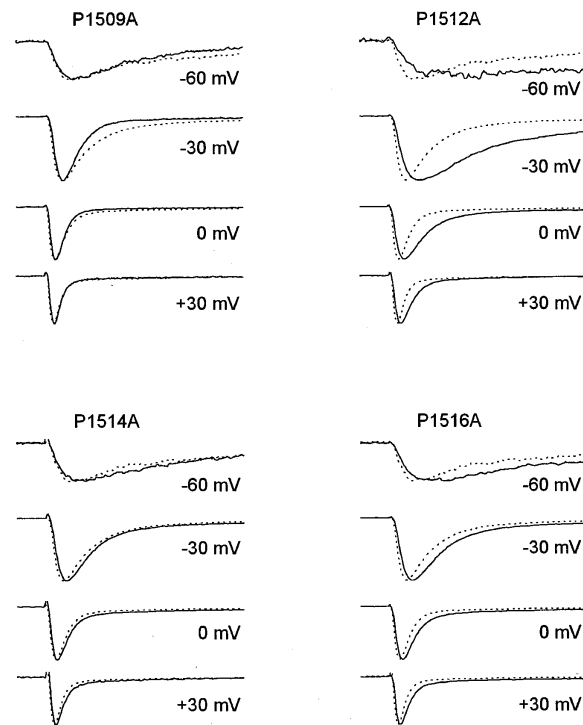


FIGURE 3. Average macropatch current traces of mutants of proline residues. Average current traces are from cell-attached macropatches, elicited by depolarizations to the potentials indicated. Current traces from different experiments were normalized and averaged. WT (dotted lines, $n = 13$); mutants (solid lines, $n = 4-16$).

fore, to understand the single channel basis for macroscopic current, it was important to consider such high P_o sweeps separately and assess their contribution to the overall behavior (e.g., Patlak and Ortiz, 1985; 1986; Bennett et al., 1995; Dumaine et al., 1996).

Sweeps were separated into two data sets depending on whether they contained high P_o behavior as indicated by bursts of activity after 8 ms of depolarization. The last traces in each panel of Fig. 5 compare ensemble averages of all the current traces analyzed (solid traces) to ensemble averages from which high P_o traces have been omitted, which therefore represent the predominant gating behavior (dashed traces). The dotted traces are ensemble averages from WT channels for comparison. For each of the mutants macroscopic inactivation due to the predominant gating behavior (dashed traces) was slower than in WT (dotted traces). The most notable effect of including high P_o sweeps was seen for mutant G1485A, where they produced a non-inactivating component that was also present in the macroscopic currents for this mutant (Fig. 1). For G1484A and P1512A, the main effects of the mutations on the macroscopic current were observed in the traces with the predominant gating behavior but were increased in magnitude by inclusion of sweeps displaying high P_o gating.

Because most aspects of macroscopic currents were reproduced by channels displaying the predominant, low P_o gating behavior, the properties of single channels during depolarizations to -20 mV were analyzed with high P_o sweeps omitted (Fig. 6). The time constants of single exponential fits to open time histograms (compared to 0.39 ms for WT, see Kellenberger

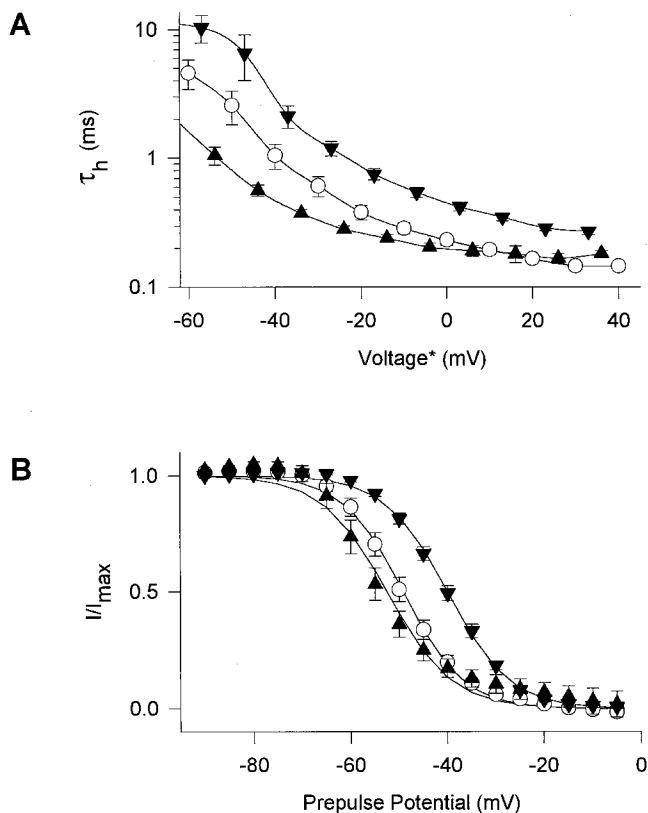


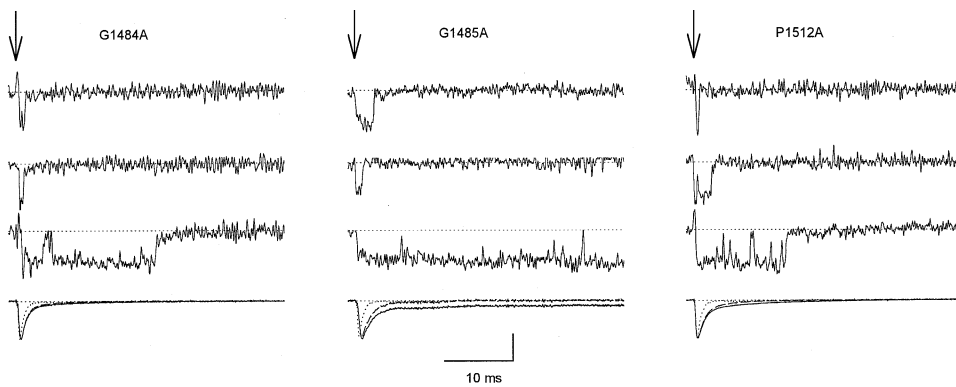
FIGURE 4. Voltage dependence of macroscopic inactivation properties of proline mutants. (A) Voltage dependence of macroscopic inactivation. τ_h was determined from single exponential fits to the current decay in macropatch experiments. Averages from 4 to 16 experiments are shown for WT (\circ), P1509A (\blacktriangle), and P1512A (\blacktriangledown). *The voltage for τ_h values of mutant channels was corrected for differences in the mean midpoints of the activation curves relative to WT. $\Delta V_{1/2}$ relative to WT in macropatch experiments was +4 mV (P1509A) and +7 mV (P1512A). (B) Steady-state inactivation curves in response to 100-ms pulses. Data are averages of 4–7 two-electrode voltage-clamp experiments (Table I) with WT (\circ), P1509A (\blacktriangle), and P1512A (\blacktriangledown). Solid lines are least-square fits of the Boltzmann equation to the data.

et al., 1997, in this issue) were 0.39 ms for G1484A and 0.59 ms for G1485A. A second component with a slower time constant represented <10% of openings in these two mutants (Fig. 6 A). The open time distribution of P1512A channels was best fitted with the sum of two exponentials with time constants 0.30 and 1.40 and approximately equal amplitudes (Fig. 6 A). Multiple open times would reflect multiple open states (Correa and Bezanilla, 1994) or the presence of undetected high P_o behavior in our sample with a longer open time. The increased open times in G1485A and P1512A are likely to contribute to the slowed macroscopic inactivation in these mutants whereas the slowed macroscopic inactivation in G1484A must be primarily due to other effects.

First latency distributions measure the probability of entering the open state after a depolarization and therefore reflect the rate of channel activation. Cumulative first latency distributions, corrected for the number of channels in the patch (Patlak and Horn, 1982; Fig. 6 B) were well-fit by a delay followed by a single exponential time course. Fit parameters for maximal open probability, time constant τ , and delay were 0.57, 0.45, and 0.30 ms for G1484A, 0.65, 0.67, and 0.26 ms for G1485A, and 0.64, 0.30, and 0.21 ms for P1512A, compared to 0.54, 0.29, and 0.27 ms for WT. Thus, in the G1484A, G1485A, and P1512A mutants, the total probability of opening was slightly higher than in WT. The time course of the first latency distribution was faster than WT for the pro mutation, due to a decrease in the lag before the exponential increase in channel opening. In contrast, channel opening was clearly slower in gly mutations, due to an increase in the time constant for first opening. This shows that the mutation of P1512 makes the channel open more easily but mutations of G1484 and G1485 make opening more difficult. The slowing of the first latency is responsible for much of the slowed macroscopic inactivation time course observed in G1484A and adds to the effect of increased open times in G1485A channels causing further slowing of macroscopic inactivation.

Pro and Gly Mutations Increase the Probability of High P_o Gating

As described above, activity in patches containing mutant channels was characterized by many sweeps with prolonged bursts which were ended by inactivation or by the end of the pulse. Depolarizing pulses with such high activity were also observed for WT channels, but far less frequently. To characterize the frequency of such behavior quantitatively, we measured the probability that a channel was open between the 5th and 40th ms of each depolarization ($P_{o(ms5-40)}$). Diaries of this probability from representative WT (2 channels/patch) and P1512A (3 channels/patch) patches are shown in Fig. 7, A–C. WT channels opened only rarely after 5 ms, and, when they did, the openings were short (Fig. 7 A). For P1512A, the frequency of high P_o activity did vary with time during an experiment. High P_o openings were either rare, similar to WT (Fig. 7 B) or occurred every few sweeps (Fig. 7 C). Once or twice during each experiment of 200–2,000 depolarizing pulses, channels switched between having rare high P_o depolarizations (Fig. 7 B) and having them occur more frequently (Fig. 7 C). Diaries of G1484A and G1485A channel activity were qualitatively similar to those shown for P1512A. The high P_o behavior occurred most often in isolated sweeps which were preceded by and followed by sweeps without bursts of activity. Therefore, if high P_o behavior represents a different



patches for single-channel traces shown were four for G1484A, two for G1485A, and three for P1512A. Ensemble averages are from all single channel traces analyzed (*solid lines*) or from traces displaying the predominant, low P_o gating behavior only (*dashed lines*). The dotted traces are WT for comparison.

FIGURE 5. Single-channel records and ensemble averages of G1484A, G1485A, and P1512A mutants. Traces of single-channel activity and ensemble averages (last trace in each column) from cell-attached patches. The arrows indicate the beginning of 40-ms depolarizations to -20 mV from a holding potential of -140 mV. The vertical calibration bar is 1 pA for single-channel traces and 0.5 pA for ensemble averages. The numbers of channels in the

mode of channel gating, the rate of leaving that mode was similar to the depolarization rate of 1/s.

Most high P_o sweeps contained single prolonged bursts of openings that were terminated by inactivation, after which the channel remained inactive (e.g., Fig. 5, trace 3 for each mutant). Thus, the relative magnitude of $P_{o(ms\ 5-40)}$ largely reflects the duration of activity before such a final inactivation event. $P_{o(ms\ 5-40)}$ was measured from more than 1,500 depolarizing pulses for WT and for each of the three mutants. The frequencies of sweeps with $P_{o(ms\ 5-40)} > 0.02$ and $P_{o(ms\ 5-40)} > 0.2$ were calculated for WT and for each of the three mutants and normalized to 1 channel/patch. $P(P_{o(ms\ 5-40)} > 0.02)$ (Fig. 7D) was more than seven times that of WT for G1484A, G1485A and P1512A. $P(P_{o(ms\ 5-40)} > 0.2)$ was 62 times greater than WT for G1484A, 184 times for G1485A, and 116 times for P1512A (Fig. 7E). Thus, the probability of sustained activity is dramatically increased over WT in all mutants tested.

Comparison of the frequencies between the different mutants supports the qualitative observation that high P_o burst duration in G1485A $>$ P1512A \cong G1484A. The bursts in G1484A and P1512A generally terminated with inactivation before the end of the pulse and led to an additional slowing of the macroscopic inactivation time course in ensemble averages (Fig. 5). Many of the bursts in G1485A continued for the duration of the 40-ms long depolarization, producing sustained current in addition to slowed macroscopic inactivation.

DISCUSSION

Five Gly and Pro Residues May Contribute to Movement of the Inactivation Gate

The hinged-lid model of Na^+ channel inactivation predicts the presence of molecular hinges in the inactiva-

tion gate which allow it to close rapidly over the intracellular mouth of the open pore during the inactivation process. Mutation of five of the eight gly and pro residues in L_{III-IV} significantly slowed macroscopic inactivation during strong depolarizations: G1484, G1485, P1512, P1514, and P1516. Single channel analysis of G1484A, G1485A, and P1512A showed that these mutant channels have increased open times (G1485A, P1512A) and latency to first opening (G1484A, G1485A). In addition, these mutant channels had a higher frequency than WT of depolarizations with a sustained high P_o . The high P_o behavior in each of these mutants is most likely due to a further dramatic decrease in the $O \rightarrow I$ transition rate. High P_o gating was reproduced by reducing the $O \rightarrow I$ transition rate in simulations of SCHEME I of Kellenberger et al. (1997) for multi-channel patches.

Gly and pro residues in L_{III-IV} are important in inherited diseases of human cardiac and skeletal muscle. Naturally occurring mutations of the gly analogous to G1484 in the skeletal muscle Na^+ channel cause Na^+ channel myotonia, a disorder characterized by an impairment of muscle relaxation (Lerche et al., 1993; Mitrović et al., 1995; for review see Barchi, 1995; Hoffman et al., 1995; Cannon, 1996). In the cardiac Na^+ channel, deletion of a pro-containing triplet of amino acids in L_{III-IV} (analogous to KPQ1508-10) causes a form of long Q-T syndrome, a disorder which increases the duration of ventricular action potentials and can cause sudden death due to ventricular arrhythmias (Bennett et al., 1995; Wang et al., 1995a, b; Dumaine et al., 1996). These mutant channels show slowed macroscopic inactivation and have a more frequent occurrence of depolarizations with high P_o activity.

Mutations of gly and pro residues in L_{III-IV} primarily cause slowing of transitions which lead to inactivation of Na^+ channels. These results are in striking contrast

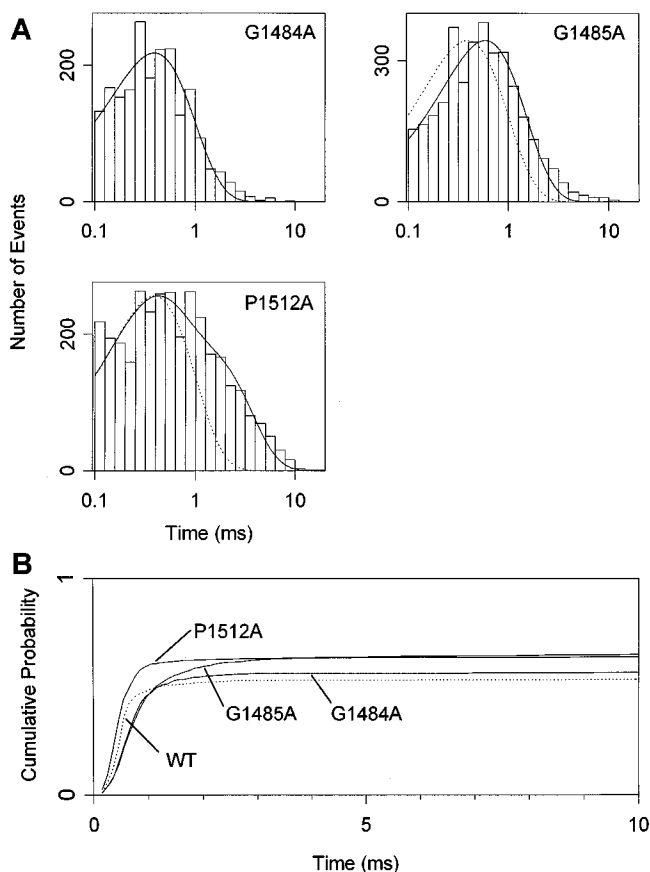


FIGURE 6. Single-channel properties of G1484A, G1485A and P1512A mutants at -20 mV. Data are from two patches for G1484A and from three patches for G1485A and P1512A. Patches containing 1–4 channels were used for the analysis. (A) Histograms of single-channel open time at -20 mV. The solid lines are fits of single exponentials (G1484A, G1485A) and of the sum of two exponentials (P1512A) to the log binned data. The time constants derived from the fits are 0.39 ms for G1484A (1,916 events analyzed), 0.59 ms for G1485A (3,374), and 0.30 and 1.40 ms with approximately equal relative amplitudes for P1512A (2,983). The dotted lines are single exponentials with the WT time constant. Mean open times for individual patches were 0.50 and 0.47 ms (G1484A), 1.66, 0.61, and 0.69 ms (G1485A) and 1.00, 0.47, and 0.78 ms (P1512A). (B) Cumulative first latency distributions at -20 mV. Distributions were corrected for the channel number (Patlak and Horn, 1982). The number of binned events was 2,316 (WT), 1,374 (G1484A), 2,257 (G1485A), and 3,422 (P1512A).

to the effects of mutations in the putative inactivation particle, including the hydrophobic IFM motif and T1491, which primarily destabilize the inactivated state and accelerate the return from the inactivated state (Kellenberger et al., 1997). Thus, these data argue for distinct roles of these two sets of amino acid residues in the inactivation process. We propose that G1484, G1485, P1512, P1514, and P1516 participate in the hinge motion that accompanies closure of the inactivation gate. No single one of these amino acid residues is absolutely

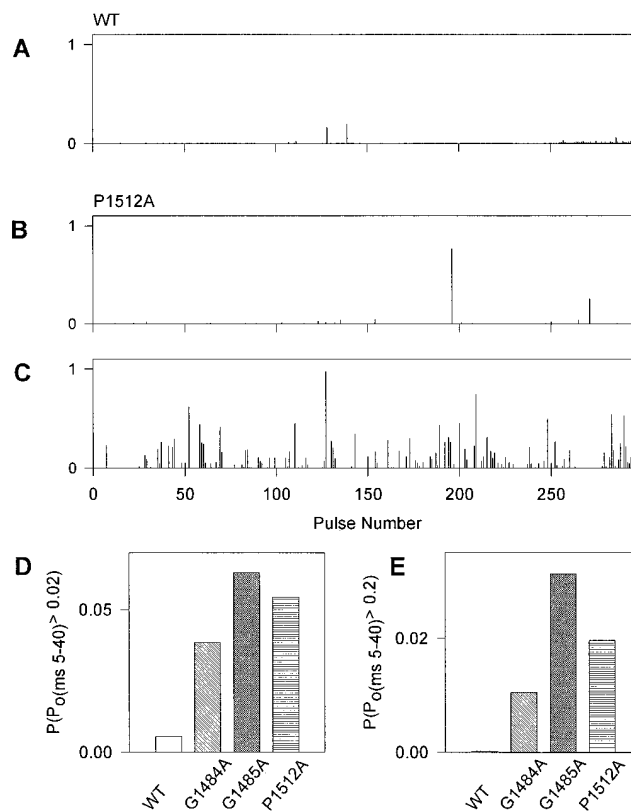
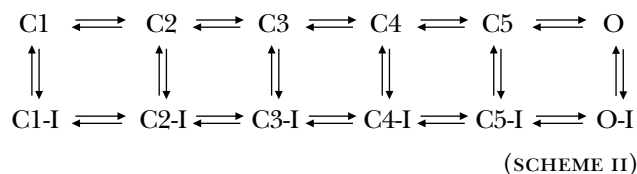


FIGURE 7. Nature and frequency of high P_o behavior in mutants G1484A, G1485A, and P1512A at -20 mV. (A–C) Diaries of activity during repetitive stimulation. P_o was measured between 5 and 40 ms of each depolarization ($P_{o(ms\ 5-40)}$) and plotted. (A) WT. (B) Behavior of P1512A when P_o was low. (C) Data obtained at a later time from the same P1512A patch when at least one channel had a higher frequency of depolarizations with high P_o . The overall frequency and pattern of depolarizations with high P_o for mutants G1484A and G1485A were similar to P1512A. (D–E) The frequency of sweeps with $P_{o(ms\ 5-40)} > 0.02$ (D) and > 0.2 (E), is plotted for WT, G1484A, G1485A, and P1512A. Data have been normalized to 1 channel/patch and were derived from 2,907 depolarizing sweeps from 2 patches (WT), 1,751 sweeps/2 patches (G1484A), 3,343 sweeps/3 patches (G1485A), and 4,003 sweeps/3 patches (P1512A).

essential for this closing motion because mutations of these single residues cause only up to threefold increases in τ_h for macroscopic inactivation at depolarized potentials and up to 14-mV positive shifts in steady state inactivation at negative membrane potentials. Evidently, multiple amino acid residues participate in the molecular rearrangements which allow closure of the inactivation gate and can compensate for single mutations of these gly and pro residues. Nevertheless, our results support the concept that amino acid residues on both sides of the inactivation particle participate in the motion required for closure of the inactivation gate and are consistent with a hinge motion for this process.

Voltage Dependence of Effects of Gly and Pro Mutations

Although the simple model of SCHEME I in the preceding paper (Kellenberger et al., 1997) is adequate for description of Na⁺ channel behavior during strong depolarizations, it is not adequate for the negative potential range because it does not contain closed inactivated states. A more realistic model (SCHEME II, Stimers et al., 1985) incorporates the possibility of inactivation from all closed states. We will use this model to discuss some of the effects of the mutations on channel gating



A feature of most mutations which slow macroscopic inactivation is that their effects are greater at more positive potentials. This behavior is expected for mutants which affect the open to inactivated transition (O → O-I in SCHEME II), which is thought to be voltage-independent (Armstrong and Bezanilla, 1977; Armstrong, 1981; Aldrich et al., 1983). In WT neuronal Na⁺ channels, the rate of activation is slower than the rate of entry into the inactivated state for small depolarizations and strongly influences the time course of macroscopic inactivation. The inactivation rate becomes rate limiting at more positive potentials, where activation is faster (Aldrich et al., 1983; Aldrich and Stevens, 1987). Inactivation of the mutant channels cannot be accelerated by stronger depolarizations, because the rate-limiting transition is voltage-independent. In contrast, the effects of the P1512A and P1509A mutations were strongest at small depolarizations (Fig. 4 A). This behavior suggests that mutations P1509A and P1512A affect voltage-dependent transitions required for inactivation. Evidence for a voltage-dependent step in inactivation also comes from studies of a mutation in the third transmembrane segment of domain IV of the human skeletal muscle Na⁺ channel α subunit (Ji et al., 1996), which slowed macroscopic inactivation with a similar voltage dependence as P1512A, and from the observation that α-scorpion toxins and sea anemone toxins immobilize a component of gating charge and cause slowed inactivation without pronounced effects on channel activation (Nonner, 1979; Neumcke et al., 1985; Hanck and Sheets, 1995; Sheets and Hanck, 1995).

Effects on Gating Transitions in Closed Channels

The mutations G1484A, G1484V, and P1512A shifted the voltage dependence of steady-state inactivation positively without affecting the rate of recovery from inactivation. Steady-state inactivation depends on rate constants for entry into and exit from inactivated states

(transitions C_n → C_n-I and C_n-I → C_n in SCHEME II). The behavior of these mutant channels is consistent with a reduction in the C_n → C_n-I transition rates, while leaving the reverse transition rates unchanged.

The mutations P1512A, G1484A, and G1485A affect the fast component of first latencies, which represents the time between depolarization and opening of the channel. Thus, these mutations affect transitions C1 ↔ C2 ↔ . . . ↔ C5 → O in SCHEME II which occur before the inactivation gate closes and binds to its receptor. The simplest interpretation of the effects on transitions in the activation pathway is that these mutations affect conformational changes in L_{III-IV} which are required for fast inactivation and also are coupled to movements of the voltage sensors and therefore are rate limiting for channel activation.

In the mutant YY1497/8QQ (Kellenberger et al., 1997), steady-state inactivation was shifted positively by 6 mV, indicating a change in the equilibrium between closed (C_n) and closed inactivated states (C_n-I). Recovery from inactivation was accelerated, indicating an increase in the rate for leaving inactivated states at negative potentials. The faster recovery of YY1497/8QQ mutant channels from inactivation indicates destabilization of the closed/inactivated states (C-I in SCHEME II) or an increase in the transition rates from the open/inactivated state back to closed/inactivated states (O-I → C₅-I → . . . → C₁-I) in response to repolarization. The mutation analogous to YY1497/8QQ in the human heart Na⁺ channel causes complete loss of the voltage dependence of the time constant for macroscopic inactivation and strong acceleration of recovery from inactivation (O'Leary et al., 1995), consistent with the conclusion that Y1497 and Y1498 are important for normal coupling of activation to inactivation in both cardiac and brain Na⁺ channels.

A Model for Na⁺ Channel Inactivation

Current models of Na⁺ channel inactivation are based on the model of Armstrong and Bezanilla (1977) which proposed that depolarization causes activation gates to move, ultimately creating a favorable binding site for a tethered cytoplasmic inactivation particle that acts as an open channel blocker. We propose the following updated version of this model. Immediately after onset of a depolarizing pulse, the channel protein including the inactivation gate L_{III-IV} undergoes conformational transitions. Activation and inactivation are coupled during transitions which precede channel opening, as indicated by the effect of mutations of G1484, G1485, F1489, T1491, and P1512 on first latency distributions. These transitions lead progressively to opening of the pore and creation of a favorable inactivation gate receptor site. Conformational changes in the inactivation gate allow its rapid movement into a closed position

and binding to the inactivation gate receptor. Two steps can be distinguished which are required for channel inactivation but not for channel opening. The first is a voltage-dependent transition made evident by mutations P1509A and P1512A in our study, by mutations in IVS3 which show a similar behavior (Ji et al., 1996), and by charge immobilization by α -scorpion and sea anemone toxins (Sheets and Hanck, 1995). The second step is the final voltage-independent closure and binding of the inactivation gate to its receptor. This voltage-independent step is affected by mutations of gly

and pro residues which contribute to the hinge-like motion of the gate. Once inactivated, the inactivation gate is bound firmly to its receptor via hydrophobic interactions with F1489 in the IFM motif and additional interactions with T1491 (West et al., 1992; Kellenberger et al., 1997). Although this "hinged-lid" model for inactivation is fully consistent with extensive electrophysiological and molecular biological results, definitive proof of this mechanism of inactivation will require structural analysis of resting and inactivated Na⁺ channels.

This research was supported by National Institutes of Health Research Grant NS 15751 to W.A. Catterall and postdoctoral fellowships from the Swiss National Science Foundation and the Schweizerische Stiftung für medizinisch-biologische Stipendien to S. Kellenberger.

Original version received 15 October 1996 and accepted version received 25 February 1997.

REFERENCES

- Aldrich, R.W., D.P. Corey, and C.F. Stevens. 1983. A reinterpretation of mammalian sodium channel gating based on single channel recording. *Nature (Lond.)* 306:436–441.
- Aldrich, R.W., and C.F. Stevens. 1987. Voltage-dependent gating of single sodium channels from mammalian neuroblastoma cells. *J. Neurosci.* 7:418–431.
- Armstrong, C.M. 1981. Sodium channels and gating currents. *Physiol. Rev.* 61:644–683.
- Armstrong, C.M., and F. Bezanilla. 1977. Inactivation of the sodium channel. II. Gating current experiments. *J. Gen. Physiol.* 70:567–590.
- Barchi, R.L. 1995. Molecular pathology of the skeletal muscle sodium channel. *Annu. Rev. Physiol.* 57:355–385.
- Bennett, P.B., K. Yazawa, N. Makita, and A.L. George. 1995. Molecular mechanism for an inherited cardiac arrhythmia. *Nature (Lond.)* 376:683–685.
- Cannon, S.C. 1996. Sodium channel defects in myotonia and periodic paralysis. *Annu. Rev. Neurosci.* 19:141–164.
- Catterall, W.A. 1992. Cellular and molecular biology of voltage-gated sodium channels. *Physiol. Rev.* 72:S15–S48.
- Correa, A.M., and F. Bezanilla. 1994. Gating of the squid sodium channel at positive potentials. II. Single channels reveal two open states. *Biophys. J.* 66:1864–1878.
- Creighton, T.E. 1993. *Proteins: Structures and molecular properties*. 2nd ed. W.H. Freeman and Company, New York, NY. 171–188.
- Derewenda, U., A.M. Brzozowski, D.M. Lawson, and Z.S. Derewenda. 1992. Catalysis at the interface: The anatomy of a conformational change in a triglyceride lipase. *Biochemistry.* 31:1532–1541.
- Dumaine, R., Q. Wang, M.T. Keating, H.A. Hartmann, P.J. Schwartz, A.M. Brown, and G.E. Kirsch. 1996. Multiple mechanisms of Na⁺ channel-linked long-QT syndrome. *Circ. Res.* 78:916–924.
- Eaholtz, G., T. Scheuer, and W.A. Catterall. 1994. Restoration of inactivation and block of open sodium channels by an inactivation gate peptide. *Neuron.* 12:1041–1048.
- Hanck, D.A., and M.F. Sheets. 1995. Modification of inactivation in cardiac sodium channels: Ionic current studies with Anthopleurin-A toxin. *J. Gen. Physiol.* 106:601–616.
- Hoffman, E.P., F. Lehmann-Horn, and R. Rüdel. 1995. Overexcited or inactive: ion channels in muscle disease. *Cell.* 80:681–686.
- Ji, S., A.L. George, R. Horn, and R.L. Barchi. 1996. Paramyotonia congenital mutations reveal different roles for segments S3 and S4 of domain D4 in hSKM1 sodium channel gating. *J. Gen. Physiol.* 107:183–194.
- Joseph, D., G.A. Petsko, and M. Karplus. 1990. Anatomy of a conformational change: hinged "lid" motion of the triosephosphate isomerase loop. *Science (Wash. DC)* 249:1425–1428.
- Kellenberger, S., T. Scheuer, and W.A. Catterall. 1996. Movement of the Na⁺ channel inactivation gate during inactivation. *J. Biol. Chem.* 271:30971–30979.
- Kellenberger, S., J.W. West, T. Scheuer, and W.A. Catterall. 1997. Molecular analysis of the inactivation particle in the inactivation gate of brain type IIA Na⁺ channels. *J. Gen. Physiol.* 109:589–605.
- Lerche, H., R. Heine, U. Pika, A.L. George, N. Mitrovic, M. Browatzki, T. Weiss, M. Rivet Bastide, C. Franke, M. Lomonaco, et al. 1993. Human sodium channel myotonia: slowed channel inactivation due to substitutions for a glycine within the III-IV linker. *J. Physiol. (Lond.)* 470:13–22.
- Mitrović, N., A.L. George, H. Lerche, S. Wagner, C. Fahlke, and F. Lehmann-Horn. 1995. Different effects on gating of three myotonia-causing mutations in the inactivation gate of the human muscle sodium channel. *J. Physiol. (Lond.)* 487:107–114.
- Neumcke, B., W. Schwartz, and R. Stämpfli. 1985. Comparison of the effects of Anemonia toxin II on sodium and gating currents in frog myelinated nerve. *Biochim. Biophys. Acta.* 814:111–119.
- Nonner, W. 1979. Effects of *Leiurus* scorpion venom on the gating current in myelinated nerve. *Adv. Cytopharmacol.* 3:345–352.
- O'Leary, M.E., L.Q. Chen, R.G. Kallen, and R. Horn. 1995. A molecular link between activation and inactivation of sodium channels. *J. Gen. Physiol.* 106:641–658.
- Patlak, J., and R. Horn. 1982. Effect of N-bromoacetamide on single sodium channel currents in excised membrane patches. *J. Gen. Physiol.* 79:333–351.
- Patlak, J.B., and M. Ortiz. 1985. Slow currents through single sodium channels of the adult rat heart. *J. Gen. Physiol.* 86:89–104.
- Patlak, J.B., and M. Ortiz. 1986. Two modes of gating during late Na⁺ channel currents in frog sartorius muscle. *J. Gen. Physiol.* 87:305–326.
- Stimers, J.R., F. Bezanilla, and R.E. Taylor. 1985. Sodium channel

- activation in the squid giant axon. Steady state properties. *J. Gen. Physiol.* 85:65–82.
- Sheets, M.F., and D.A. Hanck. 1995. Voltage-dependent open-state inactivation of cardiac sodium channels: gating current studies with Anthopleurin-A toxin. *J. Gen. Physiol.* 106:617–640.
- Vassilev, P.M., T. Scheuer, and W.A. Catterall. 1988. Identification of an intracellular peptide segment involved in sodium channel inactivation. *Science (Wash. DC)*. 241:1658–1661.
- Vassilev, P., T. Scheuer, and W.A. Catterall. 1989. Inhibition of inactivation of single sodium channels by a site-directed antibody. *Proc. Natl. Acad. Sci. USA*. 86:8147–8151.
- Wang, Q., J. Shen, Z. Li, K. Timothy, G.M. Vincent, S.G. Priori, P.J. Schwartz, and M.T. Keating. 1995a. Cardiac sodium channel mutations in patients with long QT syndrome, an inherited cardiac arrhythmia. *Hum. Mol. Genet.* 4:1603–1607.
- Wang, Q., J. Shen, I. Splawski, D. Atkinson, Z. Li, J.L. Robinson, A.J. Moss, J.A. Towbin, and M.T. Keating. 1995b. SCN5A mutations associated with an inherited cardiac arrhythmia, long QT syndrome. *Cell*. 80:805–811.
- West, J.W., D.E. Patton, T. Scheuer, Y. Wang, A.L. Goldin, and W.A. Catterall. 1992. A cluster of hydrophobic amino acid residues required for fast Na⁺-channel inactivation. *Proc. Natl. Acad. Sci. USA*. 89:10910–10914.
- Wierenga, R.K., M.E. Noble, J.P. Postma, H. Groendijk, K.H. Kalk, W.G. Hol, and F.R. Opperdoes. 1991. The crystal structure of the “open” and the “closed” conformation of the flexible loop of trypanosomal triosephosphate isomerase. *Proteins*. 10:33–49.